A Novel Rac1-GSPT1 Signaling Pathway Controls Astrogliosis Following Central Nervous System Injury*

Taiji Ishii[‡1], **Takehiko Ueyama**[‡1,2], **Michiko Shigyo**[§], **Masaaki Kohta**[¶], **Takeshi Kondoh**[¶], **Tomoharu Kuboyama**[§], **Tatsuya Uebi**[‡], **Takeshi Hamada**[‡], **David H. Gutmann**[∥], **Atsu Aiba**[**], **Eiji Kohmura**[¶], **Chihiro Tohda**[§], and **Naoaki Saito**[‡1,3]

*From the ‡Laboratory of Molecular Pharmacology, Biosignal Research Center, Kobe University, Kobe 657-8501, Japan, the §Division of Neuromedical Science, Department of Bioscience, Institute of Natural Medicine, University of Toyama, Toyama 930-0194, Japan, the ¶Department of Neurosurgery, Kobe University Graduate School of Medicine, Kobe 650-0017, Japan, the ∥Department of Neurology, Washington University School of Medicine, St. Louis, Missouri 63110, and the **Laboratory of Animal Resources, Center for Disease Biology and Integrative Medicine, Faculty of Medicine, University of Tokyo, Tokyo 113-0033, Japan*

Edited by Paul E. Fraser

Astrogliosis (*i.e.* glial scar), which is comprised primarily of proliferated astrocytes at the lesion site and migrated astrocytes from neighboring regions, is one of the key reactions in determining outcomes after CNS injury. In an effort to identify potential molecules/pathways that regulate astrogliosis, we sought to determine whether Rac/Rac-mediated signaling in astrocytes represents a novel candidate for therapeutic intervention following CNS injury. For these studies, we generated mice with Rac1 deletion under the control of the GFAP (glial fibrillary acidic protein) promoter (*GFAP-Cre;Rac1^flox/flox*). *GFAP-Cre;Rac1^flox/flox* (Rac1-KO) mice exhibited better recovery after spinal cord injury and exhibited reduced astrogliosis at the lesion site relative to control. Reduced astrogliosis was also observed in Rac1-KO mice following microbeam irradiation-induced injury. Moreover, knockdown (KD) or KO of Rac1 in astrocytes (LN229 cells, primary astrocytes, or primary astrocytes from Rac1-KO mice) led to delayed cell cycle progression and reduced cell migration. Rac1-KD or Rac1-KO astrocytes additionally had decreased levels of GSPT1 (G_1 to S phase transition 1) expression and reduced responses of IL-1β and GSPT1 to LPS treatment, indicating that IL-1β and GSPT1 are downstream molecules of Rac1 associated with inflammatory condition. Furthermore, GSPT1-KD astrocytes had cell cycle delay, with no effect on cell migration. The cell cycle delay induced by Rac1-KD was rescued by overexpression of GSPT1. Based on these results, we propose that Rac1-GSPT1 represents a novel signaling axis in astrocytes that accelerates proliferation in response to inflammation, which is one important factor in the development of astrogliosis/glial scar following CNS injury.

Astrocytes play important roles in the establishment and maintenance of numerous brain functions, including control of the blood-brain barrier; regulation of blood flow; supply of energy metabolites to neurons; synaptic function; and extracellular balance of ions, fluid, and transmitters (1). Astrocytes also respond to numerous types of CNS injury, including trauma, ischemia, infection, and neurodegenerative disease, through a process commonly referred to as astrogliosis. Astrogliosis is characterized by hypertrophic morphologic changes, accelerated proliferation, and changes in gene expression (2, 3). The degree of astrogliosis extends from reactive (transient) astrogliosis in mild cases to glial scar in severe cases (also involving microglia, fibromeningeal cells, and inflammatory cells) (2).

Rac (Rac1−3) is a member of the Rho family of small GTPases, which play fundamental roles in a wide variety of cellular processes, including transcriptional regulation, cell cycle progression, and cell migration based on actin remodeling (4, 5). In addition, Rac is an activator of three of the seven superoxide-generating NADPH oxidases (Nox; Nox1, Nox2, and Nox3)[4] (6, 7), and reactive oxygen species (ROS) generating from superoxide are detrimental factors following CNS injury (8−11). Nox2-KO mice exhibited reduced brain infarction following ischemia-reperfusion (12). Moreover, suppression of renal infarction by a dominant negative Rac1 mutant (13) and worsening of ischemia-reperfusion injury by cardiomyocyte-specific overexpression of active Rac1 have been reported (14). In astrocytes, expression of Nox2 and Nox4 has been described (15). Collectively, Rac1 is a likely candidate to mediate the cellular response to CNS injury through various cell types (including neurons and glial cells) and pathways (including actin remodeling, cell cycle progression, and Nox-derived ROS) (16). However, the effects and functions of Rac1 following CNS injury, especially in astrocytes, remain unclear.

Spinal cord injury (SCI) is a traumatic CNS injury that causes severe and persistent locomotor and sensory dysfunction (17). SCI triggers a cascade of events, including infiltration of macro-

[1] These authors contributed equally to this work.
[2] To whom correspondence may be addressed: 1-1 Rokkodai-cho, Nada-ku, Kobe 657-8501, Japan. Tel.: 81-78-803-5962; Fax: 81-78-803-5971; E-mail: tueyama@kobe-u.ac.jp.
[3] To whom correspondence may be addressed: 1-1 Rokkodai-cho, Nada-ku, Kobe 657-8501, Japan. Tel.: 81-78-803-5962; Fax: 81-78-803-5971; E-mail: naosaito@kobe-u.ac.jp.

[4] The abbreviations used are: Nox, NADPH oxidase; SCI, spinal cord injury; KD, knockdown; ROS, reactive oxygen species; BMS, Basso Mouse Scale; BSS, Body Support Scale; gbd, glass-bottomed dishes; ROI, region of interest; ANOVA, analysis of variance.

phages, leukocytes, and lymphocytes into the lesion and proliferation and migration of resident glial cells, astrocytes and microglia, around the lesion site (18, 19). During the acute phase of the injury, astrocytes increase in number and migrate to the site of the injury to isolate the inflammatory region from neighboring tissue. During the subacute and chronic phases, astrocytes form a physical barrier that is referred to as a glial scar particularly in severe SCI. The glial scar surrounding the lesion has dual effects: a beneficial effect that minimizes the inflammatory region during the acute phase of injury and a detrimental effect that restricts neuronal regeneration during the subacute and chronic phases of injury (18, 19). Thus, efficient control of the degree of astrogliosis/glial scar and appropriate timing of therapeutic intervention to astrogliosis/glial scar may be important for achieving better recovery from SCI.

To investigate whether the Rac/Rac-mediated signaling pathway in astrocytes is a novel candidate for therapeutic modalities following CNS injury, we generated astrocyte-specific Rac1-KO (*GFAP-Cre;Rac1$^{flox/flox}$*) mice. Rac1-KO mice exhibited better recovery from SCI and reduced astrogliosis following CNS injury relative to control mice. Depletion or deletion of Rac1 in astrocytes delayed cell cycle progression and reduced cell migration. We also found that the GSPT1 (G_1 to S phase transition 1) protein is a downstream molecule of Rac1 signaling in astrocytes. GSPT1/eRF3 was first identified as a molecule involved in the G_1 to S phase transition in *Saccharomyces cerevisiae* (20). Subsequently, GSPT1 was reported to mediate translation termination via the eRF1-eRF3 complex in eukaryotes (21, 22). Expression levels and responses of IL-1β and GSPT1 to LPS treatment were reduced in astrocytes with Rac1 depletion or deletion. GSPT1 depletion induced cell cycle delay, and cell cycle delay induced by Rac1 depletion was rescued by overexpression of GSPT1. Thus, we propose that Rac1-GSPT1 is a novel signaling axis that accelerates the proliferation of astrocytes during inflammation, which is one important factor in the development of astrogliosis/glial scar after CNS injury.

Results

Generation of Rac-KO Mice in Astrocytes—Among the three members of Rac, only Rac1 mRNA was detected in astrocytes by RT-PCR (Fig. 1*A*). Based on this result, we generated *Rac1*-KO mice in astrocytes using GFAP-Cre transgenic mice (23) and *Rac1$^{flox/flox}$* mice (24), hereafter referred to as *GFAP-Cre;Rac1$^{flox/flox}$* (*Rac1*-KO) mice. KO of Rac1 in astrocytes was confirmed by immunoblotting using primary astrocytes obtained from Rac1-KO mice (Fig. 1*B*). Moreover, the pattern of *GFAP-Cre*-driven recombination was assessed using *GFAP-Cre;Rac1$^{flox/+}$;tdTomato* mice generated by the intercrossing of *GFAP-Cre;Rac1$^{flox/flox}$* and *CAG-STOP^{flox};tdTomato* mice (Fig. 1, *C* and *D*). Fluorescence for tdTomato expression was positive in GFAP-positive astrocytes within the spinal cords of *GFAP-Cre;Rac1$^{flox/+}$;tdTomato* mice but not control (*Rac1$^{flox/+}$;tdTomato*) mice (Fig. 1*E*).

Better Recovery of Rac1-KO Mice after SCI—We developed SCI in Rac1-KO mice via a contusion injury and evaluated the locomotor capabilities of their hind limbs at 18 time points (1, 3, 5, 7, 9, 11, 13, 15, 17, 19, 21, 23, 25, 27, 29, 31, 33, and 35 days
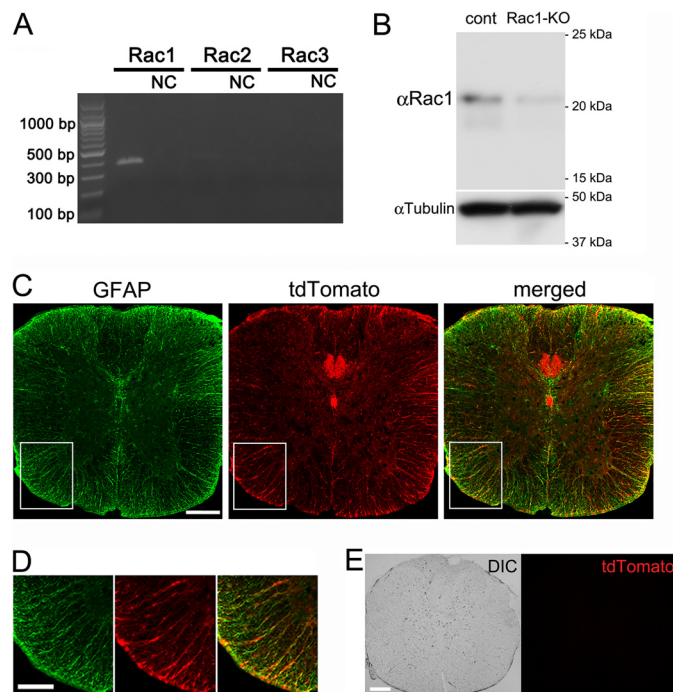

FIGURE 1. **Rac1-KO in astrocytes.** *A*, RT-PCR was performed using cDNA obtained from WT primary astrocytes and specific primer-pairs of Rac1, Rac2, and Rac3. The predicted sizes of the amplified Rac1, Rac2, and Rac3 bands are 454, 581, and 440 bp. *NC*, negative control (without cDNA). *B*, primary astrocytes obtained from control and *GFAP-Cre;Rac1$^{flox/flox}$* (Rac1-KO) mice were subjected to immunoblotting using a Rac1 antibody. Comparable loading of proteins was confirmed using tubulin-α antibody. *C*, spinal cords obtained from *GFAP-Cre;Rac1$^{flox/+}$;tdTomato* mice were subjected to immunostaining using a GFAP antibody followed by Alexa 488 secondary antibody and then observed under a confocal laser microscope. *Scale bar*, 200 μm. *D*, magnified images of the area indicated by the *rectangles* in *C* are shown. *Scale bar*, 100 μm. *E*, spinal cords obtained from control (*Rac1$^{flox/+}$;tdTomato*) mice were observed under a confocal laser microscope. *DIC*, differential interference image. *Scale bar*, 200 μm.

post-injury) over 35 days using 2 scoring systems: the 0–8-point Basso Mouse Scale (BMS) score (25) and the 0–4-point Body Support Scale (BSS) score (26). The BMS and BSS evaluate hind limb movement and body support, respectively. Recovery of locomotor capability after SCI was significantly better in Rac1-KO mice compared with control mice for both scoring systems. Better recovery in Rac1-KO mice was observed from 7 days after SCI (but not significant for BMS, $p = 0.124$). Recovery was statistically improved for both scores from 9 days after SCI until 35 days after SCI (Fig. 2*A*).

To examine histological differences between Rac1-KO mice and control mice, the spinal cord was fixed at 35 days after SCI. GFAP immunoreactivity around the injury sites (100 μm from the lesion) was significantly weaker in Rac1-KO mice compared with control mice (Fig. 2*B*). As an alternative approach to demonstrate GFAP immunoreactivity in Rac1-KO mice after CNS injury, we applied microplanar beam irradiation (100-μm width at 550 Gy with 400-μm gaps (center to center distance)) supplied from a Spring-8 synchrotron radiation facility (27) to the cerebellar cortex and brainstem. The injury caused by high energy X-rays is limited to a narrow region (27, 28). GFAP-positive immunoreactivity in a linear band surrounding the irradiated lesions was weaker in the brainstem of Rac1-KO mice compared with control mice (Fig. 2*C*). Together these
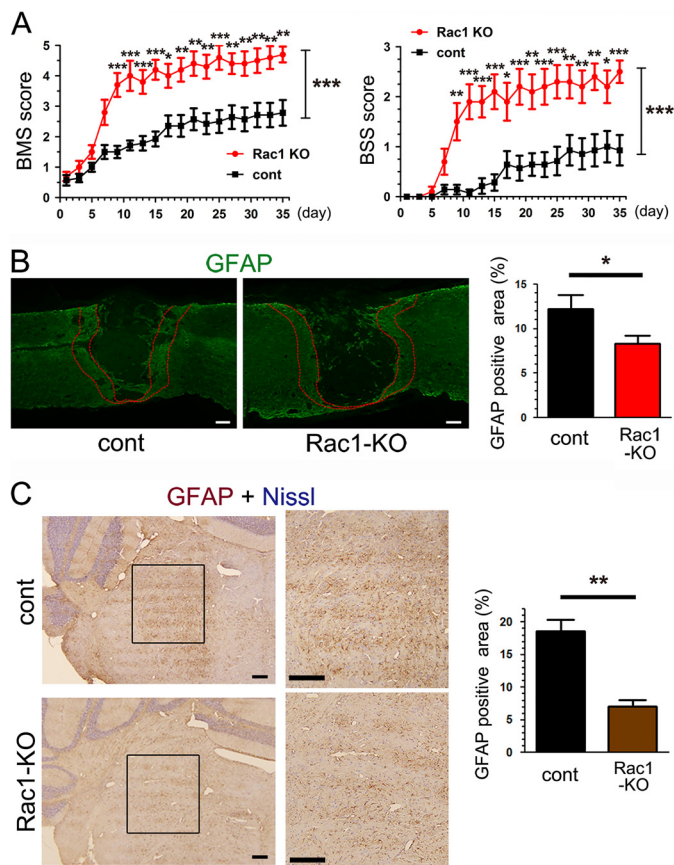
FIGURE 2. **Better recovery of locomotor function after SCI and reduced astrogliosis after CNS injuries in Rac1-KO mice.** *A*, BMS and BSS scores were recorded from days 1 to 35 after SCI. From day 9 after SCI, both hind limb movement and body support capability in Rac1-KO mice were significantly better than in control (*cont*) mice. This significant difference was sustained until day 35 (control; n = 14 hind limbs, Rac1-KO; n = 10 hind limbs; *, $p <$ 0.05; **, $p <$ 0.01; ***, $p <$ 0.001 by Bonferroni's post hoc test following two-way ANOVA). *B*, sagittal sections of spinal cords from control and Rac1-KO mice 35 days after SCI were immunostained using a GFAP antibody and Alexa 488 secondary antibody. Immunoreactivity to GFAP in the area 100-μm rostral and caudal from the edge of the lesion (indicated by *red lines*) is shown (control; n = 12 sections from 3 mice, Rac1-KO; n = 12 sections from 4 mice; *, p = 0.0420). *Scale bars*, 100 μm. *C*, coronal sections of the right cerebellum and brainstem from control and Rac1-KO mice 21 days after microbeam irradiation injury (horizontally propagating multibeams, 100-μm width with 400-μm gaps between them) were immunostained using a GFAP antibody. GFAP-positive immunoreactivity in a linear band surrounding the irradiated lesions of the brainstem is shown (control; n = 9 ROIs from 3 mice, Rac1-KO; n = 9 ROIs from 3 mice; **, p = 0.0046). The *right panels* are magnified images of the regions indicated by the *rectangles* in the *left panels*. *Scale bars*, 500 μm.

results strongly suggest that immunoreactivity to GFAP, namely astrogliosis, after CNS injury was reduced by Rac1-KO in astrocytes.

Reduced Proliferation and Migration in Rac1-KD and Rac1-KO Astrocytes—We hypothesized that reduced GFAP immunoreactivity in two different CNS-injury models is due to the reduced proliferation and/or migration following Rac1-KO in astrocytes, thereby leading to reduced astrogliosis. To examine the contribution of Rac1 to cell cycle progression and cell migration, we used the Fucci system (29) and scratch wound assay, respectively, under a long term, time lapse live-imaging system.

Rac1-KD in LN229 cells, a cell line derived from a human glioblastoma, was achieved using a verified plasmid expressing

shRNA for Rac1 (6) (Fig. 3*A*). Cell cycle progression, defined as the time from one cytokinesis to another cytokinesis, was significantly longer in Rac1-KD LN229 cells than in control cells (29.95 ± 0.66 h *versus* 36.58 ± 1.56 h; Fig. 3*B*). the G_1 phase was significantly extended by Rac1-KD (14.60 ± 1.09 h *versus* 19.64 ± 1.87 h); however, the S-M phase, defined by the green fluorescence of Venus-tagged hGeminin, was not changed by Rac1-KD (Fig. 3*B*).

Cell migration, evaluated using the scratch wound assay, was also significantly reduced in Rac1-KD LN229 cells compared with control cells (168.7 ± 21.8 μm *versus* 40.6 ± 7.3 μm) (Fig. 3*C*). Both delayed cell cycle progression and reduced cell migration were also observed in Rac1-KD primary astrocytes (cell cycle: 24.00 ± 1.04 h *versus* 31.03 ± 1.72 h, cell migration: 187.8 ± 14.7 μm *versus* 102.9 ± 7.4 μm) and in primary astrocytes obtained from Rac1-KO mice (cell cycle: 20.11 ± 0.77 h *versus* 27.59 ± 1.12 h, cell migration: 349.1 ± 12.9 μm *versus* 172.3 ± 11.4 μm) (Fig. 4, *A*–*C*). The reduced cell migration in Rac1-KO primary astrocytes was confirmed using a CytoSelect cell migration assay kit (Fig. 4*D*).

GSPT1 Is a Downstream Effector of Rac1 Signaling—LPS has been reported to induce Rac1-mediated up-regulation of various proteins, including the pro-inflammatory cytokine IL-1β (30). IL-1β is a key driver of inflammatory response and astrogliosis induced by brain damage, including SCI (31) and ischemic brain injury (32). First, we confirmed increased protein levels of IL-1β following LPS treatment in primary astrocytes from WT mice, as well as reduced IL-1β expression following LPS treatment in primary astrocytes from Rac1-KO mice. These findings indicate the existence of a Rac1-dependent transcriptional pathway enhanced by LPS treatment (Fig. 5*A*). Second, to identify novel downstream molecules in Rac1 signaling associated with the cell cycle and cell migration, we performed a DNA microarray using control and Rac1-KD LN229 cells treated with LPS (Fig. 5*B*), from which reduced levels of GSPT1 in Rac1-KD cells were detected compared with control cells. Decreased protein levels of GSPT1 were confirmed in LN229 cells using two different siRNAs for Rac1, as well as from primary astrocytes from Rac1-KO mice (Fig. 5*C*). In addition, GSPT1 was increased after treatment with LPS, and the decreased expression of GSPT1 following LPS treatment was observed in Rac1-KD LN229 cells (Fig. 5*C*). Furthermore, the increase in GSPT1 levels following LPS treatment was inhibited by a JNK inhibitor (JNK-IN-8), an ERK inhibitor (U0126), and an NF-κB inhibitor (BAY 11-7085), but not by a p38 MAP kinase inhibitor (SB203580) (Fig. 5*E*). These results suggest that GSPT1 is transcriptionally regulated by Rac1 through the activation of at least JNK, ERK, and NF-κB and that GSPT1 is up-regulated and continues to function after CNS injury, which induces inflammation.

The Rac1-GSPT1 Signaling Axis Is Involved in the Cell Cycle but Not Cell Migration—To examine the role of Rac1 and GSPT1 in cell cycle progression, we analyzed the cell cycle under long term, time lapse live-imaging in HeLa cells (another cell line rather than LN229). The cell cycle of HeLa cells was significantly prolonged following KD using two different siRNAs for GSPT1 (control: 18.47 ± 0.36 h, si620: 22.93 ± 0.40 h, and si1374: 23.25 ± 0.61 h) (Fig. 6, *A* and *B*). Further-
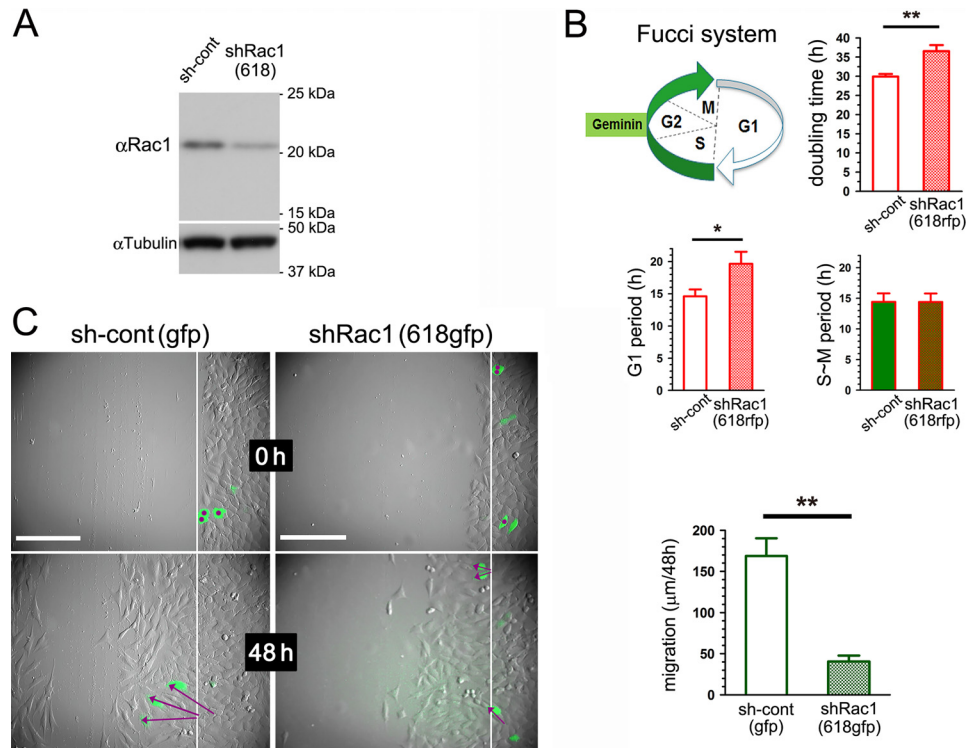
FIGURE 3. **Delayed cell cycle and impaired migration in Rac1-KD LN229 astrocytic cells.** *A*, 48 h after transfection of LN229 cells (*pSUPER* (*sh-cont*) or *shRac1(618)*), efficacy of *shRac1(618)* on Rac1 expression levels was evaluated using a Rac1 antibody. Comparable loading of proteins was confirmed using a tubulin-α antibody. *B*, from 24 to 96 h after transfection (*pSUPER(rfp)* (*sh-cont*) or *shRac1(618rfp)*), the cell cycle of the RFP-expressing cells was evaluated using a Fucci system (*upper left panel*) and an LCV110 microscope. The cell cycle time (*i.e.* doubling time) is shown in the *upper right panel* (control: $n = 57$, Rac1-KD: $n = 39$; **, $p = 0.0003$). The *lower left panel* shows the cell cycle time of the G_1 phase (control: $n = 15$, Rac1-KD: $n = 16$). The *lower right panel* shows the cell cycle time from the S to M phase (control: $n = 15$, Rac1-KD: $n = 16$; *, $p = 0.0292$). *C*, from 48 to 96 h after transfection (*pSUPER(gfp)* (*sh-cont*) or *shRac1(618gfp)*), migration capabilities of the GFP-expressing cells were monitored using an LCV110 microscope (0 h: starting time point, 48 h: ending time point, control: $n = 17$, Rac1-KD: $n = 31$; **, $p < 0.0001$). The *white lines* are located at the same position at time 0 and 48 h to show the movement (indicated by *purple arrows* at 48 h) of the cells marked by filled *purple circles* at 0 h. *Scale bar*, 200 μm.

more, the prolonged cell cycle induced by Rac1-KD (2.5 nM: 22.05 ± 0.38 h, 5 nM: 22.38 ± 0.44 h) in HeLa cells was ameliorated by overexpression of GFP-tagged GSPT1 (GFP-GSPT1) (2.5 nM: 19.73 ± 0.48 h, 5 nM: 19.76 ± 0.41 h) (Fig. 6, *C* and *D*). The delayed cell cycle progression was also observed in GSPT1-KD primary astrocytes (20 nM; control: 24.02 ± 0.82h, si620m: 28.74 ± 0.86 h; Fig. 6, *E* and *F*).

To determine whether GSPT1 controls cell migration, we employed a scratch wound assay. Cell migration was not affected by two siRNAs for GSPT1 in LN229 cells (Fig. 7, *A* and *B*). The absence of an effect of GSPT1-KD on cell migration in primary astrocytes was also confirmed using a CytoSelect cell migration assay kit (20 nM of si-cont and siGSTP1–620m; Figs. 7, *C* and *D*). These results suggest that GSPT1 is a downstream effector in Rac1 signaling and that the Rac1-GSPT1 signaling axis is involved in cell cycle regulation but not cell migration.

Discussion

Although current evidence suggests that astrogliosis is beneficial during the initial/early/acute stages of CNS injury by isolating the lesion from inflammation, astrogliosis is detrimental at later/chronic stages of injury because of inhibition of neural regeneration (18). Activation of astrocytes, which results in glial scar after severe CNS injury, starts with immediate infiltration of macrophages/leukocytes/lymphocytes to the lesion

and activation of microglia. However, this activation persists longer than those reactions to isolate and sequester the inflammation (18).

In the present study, Rac1-KO mice exhibited better functional recovery than control mice, starting from 7 days after SCI (statistically significant from 9 days after SCI) until 35 days after SCI (Fig. 2A). Rac1-KO mice also exhibited mild suppression of astrogliosis at 35 days following SCI compared with control mice. In contrast, severely reduced astrogliosis after SCI was reported in conditional STAT3-KO mice, resulting in remarkably worse motor deficits than control mice (33, 34). Thus, mildly suppressed astrogliosis may lead to reduced detrimental effects of astrogliosis during the chronic stages of SCI. In addition to mildly suppressed astrogliosis at 35 days after SCI in Rac1-KO mice, Rac1-KO astrocytes also exhibited reduced production of IL-1β following LPS treatment. Inhibition of C5aR, a G-protein-coupled receptor for complement protein C5a, was reported to have dual effects on locomotor recovery after SCI: a beneficial effect in the first 7 days after SCI by inhibiting production of various pro-inflammatory cytokines, including IL-1β, and a detrimental effect after the first 7 days by inhibiting astrogliosis (35). Thus, better functional recovery after SCI in Rac1-KO mice may be due to the dual beneficial effects of Rac1 against inflammation in the acute/subacute phase and astrogliosis in the subacute/chronic phase.
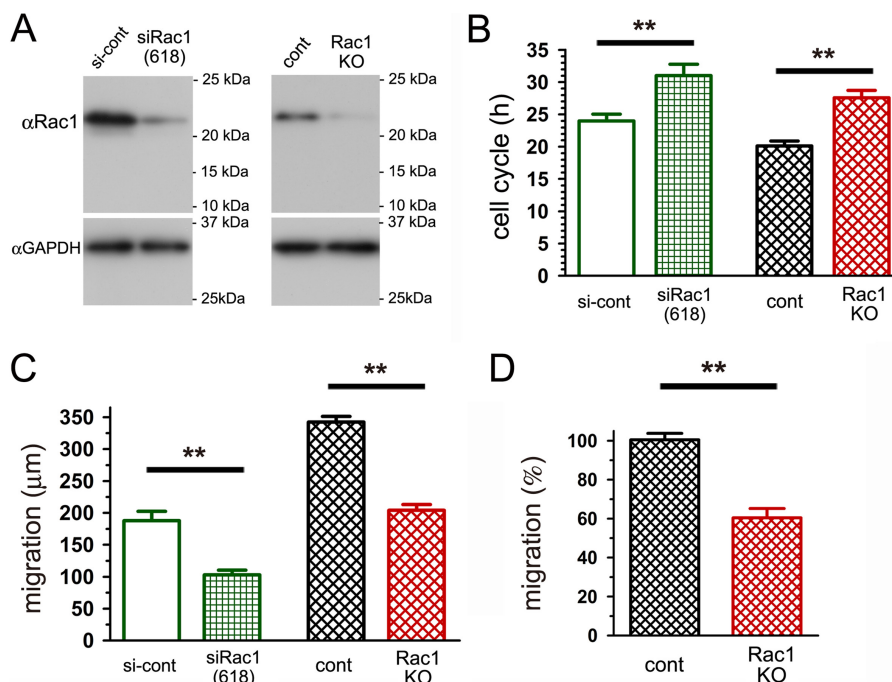
FIGURE 4. **Delayed cell cycle and impaired migration in both Rac1-KD and Rac1-KO primary astrocytes.** *A*, *left panel*, 60 h after electroporation of 20 nM siRNA (si-cont or siRac1(618) + GFP plasmid) into WT primary astrocytes, Rac1 expression levels were evaluated using a Rac1 antibody. Comparable loading of proteins was confirmed using a GAPDH antibody. *Right panel*, primary astrocytes obtained from *Rac1flox/flox;tdTomato* (control, *cont*) and *GFAP-Cre;Rac1flox/flox; tdTomato* (Rac1-KO) mice were subjected to immunoblotting using a Rac1 antibody. Comparable loading of proteins was confirmed using a GAPDH antibody. *B*, the cell cycle was evaluated using an LCV110 microscope from 48 to 120 h after electroporation in the experiment using WT primary astrocytes (siRNA + GFP plasmid) or after the preparation on a glass-bottomed dish in the experiment using primary astrocytes from Rac1-KO (with tdTomato) and control mice. The *left pair* and the *right pair* in the graph show data obtained using Rac1-KD astrocytes (control: $n = 79$, Rac1-KD: $n = 40$; **, $p = 0.0003$) and using Rac1-KO astrocytes (control: $n = 80$, Rac1-KO: $n = 82$; **, $p < 0.0001$), respectively. *C*, 48–120 h after electroporation in the experiment using WT primary astrocytes (siRNA + GFP plasmid) or in the preparation on the glass-bottomed dish in the experiment using primary astrocytes from Rac1-KO (with tdTomato) and control mice, cell migration capabilities were evaluated using an LCV110 microscope. The *left pair* and the *right pair* in the graph show data obtained using Rac1-KD astrocytes (control: $n = 31$, Rac1-KD: $n = 65$; **, $p < 0.0001$) and using Rac1-KO astrocytes (control: $n = 47$, Rac1-KO: $n = 39$; **, $p < 0.0001$), respectively. *D*, 24 h after preparing the primary astrocytes from control and Rac1-KO mice in 24-well insets, cell migration capabilities were assayed using a CytoSelect migration assay kit (control: $n = 10$, Rac1-KO: $n = 6$; **, $p < 0.0001$).

The main compartment of the glial scar is believed to be formed by proliferated astrocytes around the lesion, as well as infiltrating astrocytes from neighboring regions (18, 33). In contrast, using a stab wound cortical injury model, which is probably a weaker injury than SCI or brain infarction, Bardehle *et al.* (36) have shown that astrogliosis is not associated with astrocyte migration from neighboring regions. In addition, the authors report that astrocyte proliferation in the specific juxtavascular niche in the brain parenchyma may play important roles in astrogliosis. Although further study is required for conclusions regarding the contribution of astrocyte migration from neighboring regions in astrogliosis after SCI or brain infarction, in the present study, we found that Rac1 regulates both the proliferation and migration of astrocytic cells. Involvement of Rac1 in cell migration is well studied (37, 38); however, the precise mechanism regulating cell proliferation by Rac1 remains unclear. Although Rac1 was reported to be a negative regulator in cytokinesis (39, 40), we found delayed cell cycle progression, in particular an elongated G_1 phase, induced by Rac1-KD. Promotion of G_1 to S phase transition by Rac1 was reported to be regulated via increased levels of cyclin D1 (41, 42) through either NF-κB-dependent (5, 43) or independent (44) mechanisms. Chauvin *et al.* (45) reported that GSPT1 depletion induced decreased levels of cyclin D1 by inhibition of translation initiation via the mTORC1 pathway, which pro-

motes translation initiation rather than inhibition of translation termination. Although the precise mechanism responsible for the Rac1 control of GSPT1 levels is still unknown, GSPT1 may be transcriptionally regulated by Rac1 through the activation of JNK, ERK, and NF-κB, but not p38 MAP kinase. Thus, the Rac1-GSPT1 signaling axis plays a critical role for astroglial growth.

In addition to the involvement of GSPT1 in the cell cycle, GSPT1 has been reported to be involved in cell migration (46, 47). However, no effect of GSPT1 KD on cell migration was observed in the present study. The reason for the discrepancy between the present study and previous reports is unknown but may be due to the specific cell lines used. Xiao *et al.* (47) reported that HCT116 colorectal cancer cells exhibited high level expression of GSPT1. Given the significant reduction of migration in Rac1-KD/KO, but not GSPT1-KD, astrocytes, GSPT1 is unlikely to be involved in cell migration in this context.

Rac1 is a known tumor progression factor because of its roles in cell migration/invasion and cell proliferation (48, 49). Recently, several activating mutations of RACs, including RAC1 and RAC2, have been reported as oncogenic driver genes in human melanoma and cancer cell lines (50–52). More recently, genome-wide association studies have shown that testicular germ cell tumors are susceptible to increased GSPT1
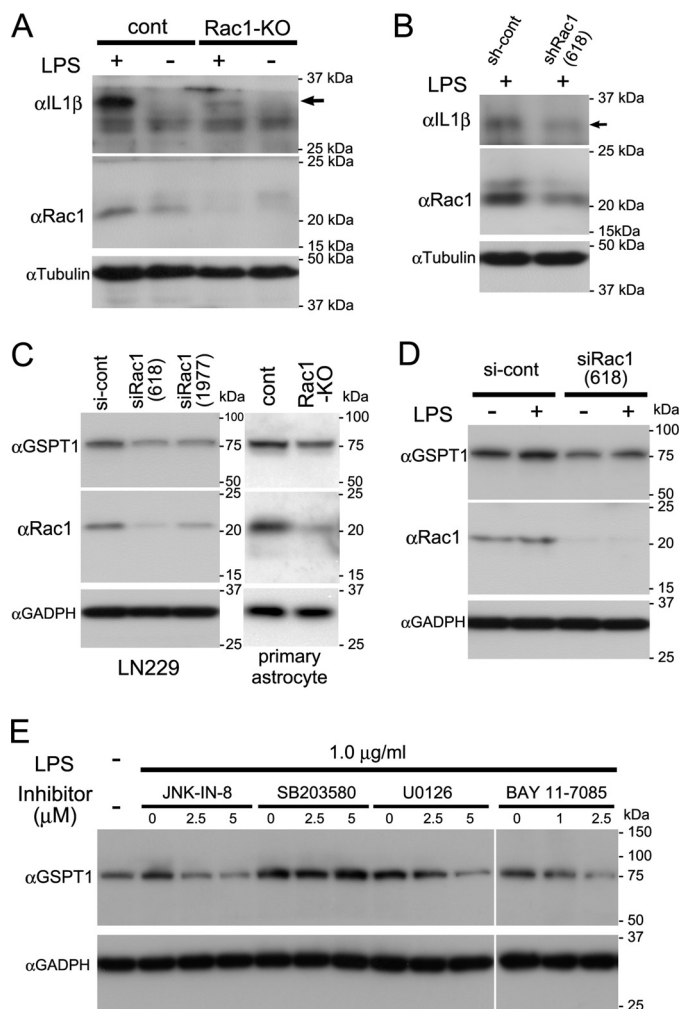
FIGURE 5. **Reduced expression of GSPT1 in Rac1-KD and -KO astrocytes.** *A*, primary astrocytes obtained from control and Rac1-KO mice were treated with or without LPS (0.5 μg/ml) for 24 h. Expression levels of IL-1β were evaluated by immunoblotting using an IL-1β antibody. Rac1-KO and comparable loading of proteins were confirmed using a Rac1 antibody and tubulin-α antibody, respectively. The *arrow* indicates the IL-1β bands. *B*, LN229 astrocytic cells transfected with *pSUPER* (sh-cont) or *shRac1(618)* were treated with LPS (0.5 μg/ml) for 24 h. Reduced expression levels of Rac1 and IL-1β and comparable loading of proteins were confirmed using a Rac1 antibody, IL-1β antibody, and tubulin-α antibody, respectively. The *arrow* indicates the IL-1β bands. *C*, Rac1 was knocked down via transfection of 2.5 nM of siRNAs (si-cont, siRac1(618), or siRac1(1977)) in LN229 cells. Primary astrocytes were prepared from control and Rac1-KO mice. Reduced expression levels of GSPT1 were evaluated using a GSPT1 antibody. Rac1-KD/KO and comparable loading of proteins were confirmed using a Rac1 antibody and GAPDH antibody, respectively. *D*, 2.5 nM of siRNAs (si-cont or siRac1(618)) were transfected in LN229 cells 24 h prior to LPS treatment. After LPS treatment (0.5 μg/ml) for 24 h, GSPT1 levels were evaluated using a GSPT1 antibody. Rac1-KD and comparable loading of proteins were confirmed using a Rac1 antibody and GAPDH antibody, respectively. *E*, LN229 cells were simultaneously treated with LPS (1.0 μg/ml) and one of four inhibitors at the indicated concentrations (μM; JNK-IN-8, SB203580, U0126, or BAY 11-7085) for 16 h. After the treatment, GSPT1 levels were evaluated using a GSPT1 antibody. Comparable loading of proteins was confirmed using a GAPDH antibody.

expression (53). Given the novel Rac1-GSPT1 signaling axis found in the present study, GSPT1 may participate in an oncogenic mechanism as a downstream target of active RAC1.

Although Rac1-GSPT1 signaling is involved in cell cycle progression from G₁ to S phase, namely cell proliferation, this involvement does not seem to explain the entirety of the effects of Rac1 on better recovery of Rac1-KO mice after SCI. Cooney

et al. (54) reported that the Nox that is most responsive in astrocytes and microglia after SCI is Nox2, a Rac1-activated Nox; in contrast, the expression of Nox4, a Rac-independent Nox, was constant over time in astrocytes. The group reported an increase in Nox2 in astrocytes at 24 h and 7 days after SCI, as well as reduced expression of pro-inflammatory cytokines via the systemic administration of a Nox2 inhibitor (54). Thus, Rac-activated Nox2 in astrocytes may be one factor that induces better recovery of Rac1-KO mice after SCI.

In summary, we found that a mild suppression of astrogliosis promotes better functional recovery after SCI and that Rac1 in astrocytes is a potential target for developing new therapeutic modalities for CNS injury. Moreover, we identified GSPT1 as a novel downstream target of Rac1 that promotes cell proliferation through the progression of the G₁ to S phase transition. GSPT1 may be a more powerful target for cancer therapy in addition to therapy against CNS injury. Further study will be required to define the precise mechanisms by which Rac1 regulates GSPT1.

Experimental Procedures

Animals—All animal experiments were conducted in accordance with Kobe University and University of Toyama guidelines. *GFAP-Cre* mice (23) and *Rac1^{flox}* mice (24) have been described previously. *GFAP-Cre;Rac1$^{flox/+}$* progeny of *Rac1$^{flox/flox}$* and *GFAP-Cre* mice were back-crossed with *Rac1$^{flox/flox}$* to obtain *GFAP-Cre;Rac1$^{flox/flox}$* (hereafter referred to as Rac1 KO) mice, which were backcrossed to *Rac1$^{flox/flox}$* to generate the *GFAP-Cre;Rac1$^{flox/flox}$* and *Rac1$^{flox/flox}$* experimental mice. *CAG-STOP^{flox}–tdTomato* (Ai9) mice, in which the ROSA26 region was used for transgene insertion, were purchased from The Jackson Laboratory (Bar Harbor, ME). *GFAP-Cre;Rac1$^{flox/+}$;tdTomato* progeny of *GFAP-Cre;Rac1$^{flox/flox}$* and *CAG-STOP^{flox}-tdTomato* mice were used to examine the efficacy of the GFAP promoter in astrocytes of the spinal cord. The *GFAP-Cre;Rac1$^{flox/+}$;tdTomato* mice were back-crossed with *Rac1$^{flox/flox}$* to obtain *GFAP-Cre;Rac1$^{flox/flox}$;tdTomato* mice, which were then backcrossed to *Rac1$^{flox/flox}$* to generate the *GFAP-Cre;Rac1$^{flox/flox}$;tdTomato* and *Rac1$^{flox/flox}$;tdTomato* experimental mice. Astrocytes obtained from *GFAP-Cre;Rac1$^{flox/flox}$;tdTomato* mice are labeled with tdTomato fluorescence, which is a marker of Rac1-KO. Control astrocytes obtained from *Rac1$^{flox/flox}$;tdTomato* mice are negative for tdTomato fluorescence and are thus not Rac1-KO cells. Offspring were genotyped by PCR using the following primers: 5′-ACTCCTTCATAAAGCCCTCG-3′ and 5′-ATCACTCG-TTGCATCGACCG-3′ for *GFAP-Cre*; 5′-ATTTTCTAGAT-TCCACTTGTGAAC-3′ and 5′-ATCCCTACTTCCTTC-CAACTC-3′ for *Rac1^{flox}*; 5′-GGCATTAAAGCAGCG-TATCC-3′ and 5′-CTGTTCCTGTACGGCATGG-3′ for tdTomato. WT C57BL/6 mice were purchased from Clea Japan.

SCI Model Experiments—14–20-week-old Rac1 KO mice and control mice were used. The mice were anesthetized via the administration of trichloroacetaldehyde monohydrate (500 mg/kg, i.p.). After the mice had completely lost their righting reflex, surgical procedures to produce SCI were performed, as described previously (26) with slight modifications. Contusion
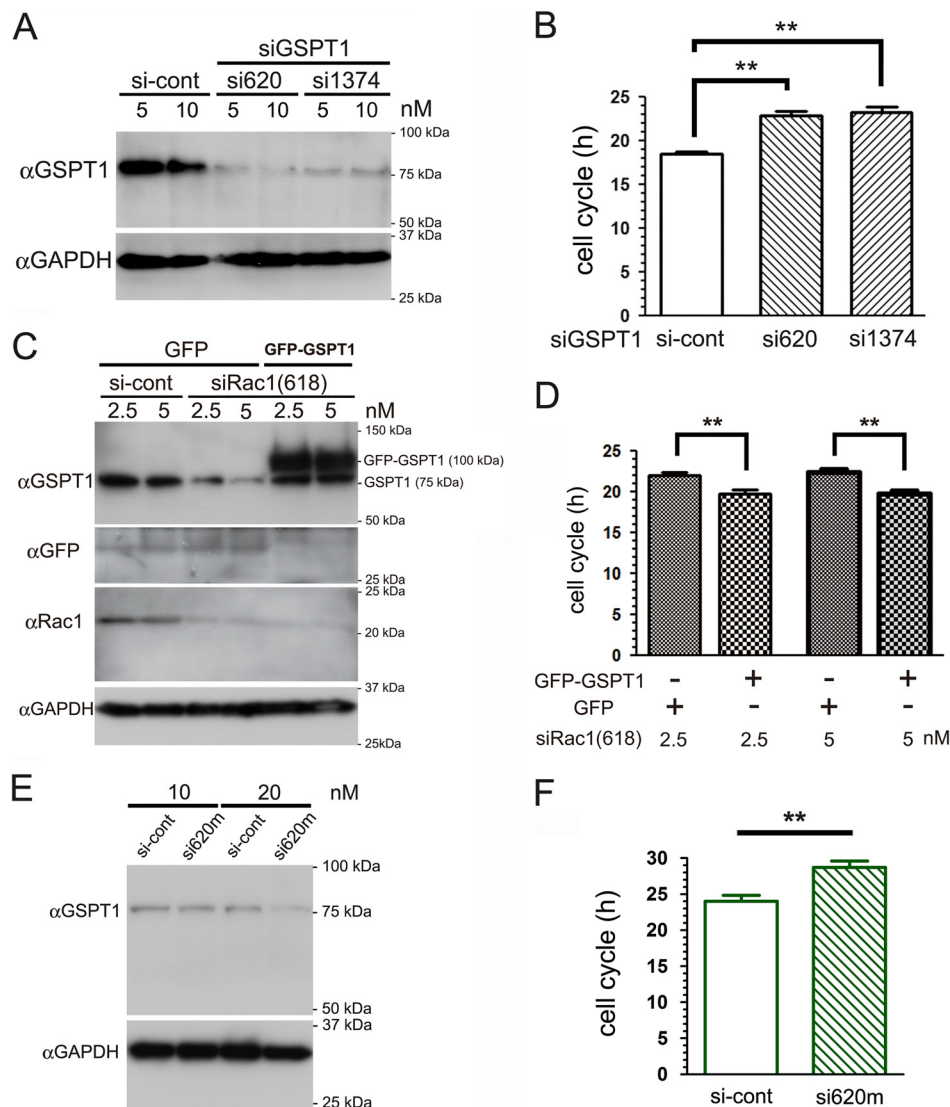
FIGURE 6. **Cell cycle delay by GSPT1-KD and rescue of cell cycle delay induced by Rac1-KD via overexpression of GSPT1.** *A*, 5 and 10 nM of control (si-cont) or two GSPT1 siRNAs (si620 or si1374) were co-transfected with Venus-hGeminin plasmid into HeLa cells. At 48 h after transfection, expression levels of GSPT1 were evaluated using a GSPT1 antibody. Comparable loading of proteins was confirmed using a GAPDH antibody. *B*, 14–96 h after transfection (10 nM of siRNA + Venus-hGeminin plasmid) into HeLa cells, the cell cycle time of Venus-hGeminin transfected cells was observed under an LCV110 microscope (si-cont: $n = 68$, si620: $n = 85$, si1374: $n = 56$; **, $p < 0.0001$). *C*, 2.5 and 5 nM of si-cont or siRac1(618) was co-transfected with the GFP plasmid into HeLa cells. For the rescue experiment, Rac1 siRNA + GFP-GSPT1 plasmid was co-transfected into HeLa cells. At 48 h after transfection, expression levels of Rac1, GSPT1, overexpressed GFP-GSPT1, and GFP were examined by immunoblotting using a Rac1, GSPT, and GFP antibody, respectively. Comparable loading of proteins was confirmed using a GAPDH antibody. *D*, from 24 to 96 h after transfection (siRac1(618) + GFP or GFP-GSPT1 plasmid) into HeLa cells, the cell cycle time of GFP or GFP-GSPT1 transfected cells was observed under an LCV110 microscope (2.5 nM siRac1, GFP: $n = 171$, GFP-GSPT1: $n = 171$; **, $p = 0.0003$; and 5 nM siRac1, GFP: $n = 148$, GFP-GSPT1: $n = 77$; **, $p < 0.0001$). *E*, 10 and 20 nM of si-cont or siGSPT1(620m) were co-electroporated with the GFP plasmid into the primary astrocytes. 60 h after electroporation, the expression levels of GSPT1 were evaluated using a GSPT1 antibody. Comparable loading of proteins was confirmed using a GAPDH antibody. *F*, from 48 to 120 h after electroporation (20 nM of siRNA + GFP plasmid) of WT primary astrocytes, the cell cycle time of the GFP-transfected cells was assessed using an LCV110 microscope (si-cont: $n = 107$, si620m: $n = 90$; **, $p = 0.0001$).

injuries were produced by dropping a 6.5-g weight from a height of 7 mm once onto the exposed dura mater of the lumbar L1 level of the spinal cord using a stereotaxic instrument (Narishige, Tokyo, Japan). The mice were allowed to recover for 35 days. For behavioral scoring, the mice were placed individually in an open field (23.5 cm × 16.5 cm × 12.5 cm) and observed for 5 min. Open field locomotion focused on each hind limb was evaluated using the 0–8-point BMS locomotion scale (25) and the 0–4-point BSS locomotion scale (26).

Microplanar Microbeam Irradiation at SPring-8—8–12-week-old Rac1-KO mice and control mice were used. The SPring-8 synchrotron facility (Japan Synchrotron Radiation Research Institute, RIKEN, Sayo, Japan) was used to supply microplanar beam irradiation. The radiation beam traveled in a vacuum transport tube with minimized air scattering of the primary beam. X-rays were emitted from the vacuum tube into the atmosphere after first passing through a beryllium vacuum window and then into a 2.0-m helium beam path consisting of an aluminum tube and a thin aluminum helium window located 42 m from the synchrotron radiation output. The sample positioning system was placed 2.5 m from the thin aluminum window. This beamline produces nearly parallel X-rays, and the mice were irradiated at a position 2.5 m from the thin aluminum window. White beam X-rays with an energy level of ∼100
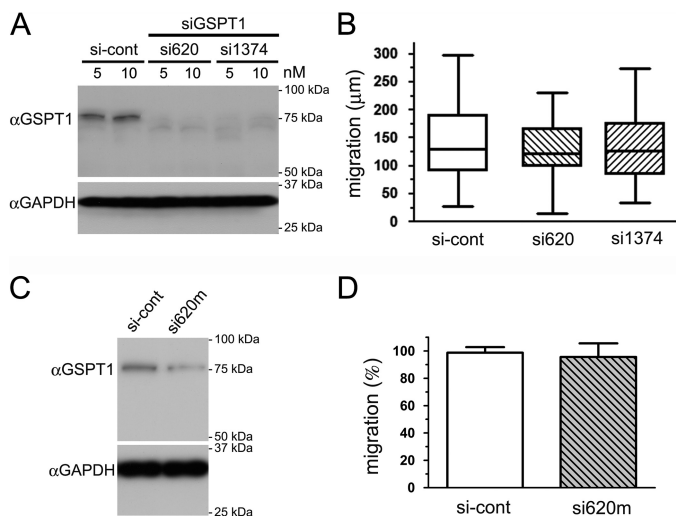
FIGURE 7. No effect of GSPT1-KD on astrocyte migration. *A,* 5 and 10 nM of control (si-cont) or two GSPT1 siRNAs (si620 or si1374) were co-transfected with GFP plasmid into LN229 astrocytic cells. At 48 h after transfection, expression levels of GSPT1 were evaluated using a GSPT1 antibody. Comparable loading of proteins was confirmed using a GAPDH antibody. *B,* from 48 to 96 h after transfection (10 nM of siRNA + GFP), the cell migration capabilities of the LN229 cells were monitored using an LCV110 microscope (si-cont: *n* = 51, si620: *n* = 50, si1374: *n* = 50). *C,* 20 nM of si-cont or siGSPT1(620m) was co-electroporated with the GFP plasmid into WT primary astrocytes. 32 h after electroporation, the expression levels of GSPT1 were evaluated using a GSPT1 antibody. Comparable loading of proteins was confirmed using a GAPDH antibody. *D,* 32 h after electroporation (20 nM of siRNA + GFP plasmid) into WT primary astrocytes, cell migration capabilities were assayed using a Cyto-Select migration assay kit (si-cont: *n* = 8, si620m: *n* = 4).

keV were derived through 3-mm Cu absorbance. The mice were irradiated with a single slit collimator at the same beam-line, with multiple horizontal microplanar beams 100-μm thick at an extremely high dose of 550 Gy with 400-μm gaps between beams on the brain. Anesthetized mice were positioned horizontally in front of the horizontally propagating beams, with the right brain aligned perpendicular to the direction of the beam. The multislit collimator, which produces 10 peak dose areas composed of 100-μm width with 400-μm gaps between them to process the microplanar beam, was set downstream of the output of the beamline hatch. The details of this multislit irradiation system have been described previously (28).

Chemicals and Antibodies—LPS was obtained from Invivo-Gen (San Diego, CA). JNK-IN-8 (Millipore, Billerica, MA), a JNK inhibitor; SB203580 (Cell Signaling Technology, Danvers, MA), a p38 MAP kinase inhibitor; U0126 (Cell Signaling Technology), an ERK inhibitor; and BAY 11-7085 (Wako Pure Chemical Industries, Japan), an NF-κB inhibitor were purchased from the respective vendors. The following specific antibodies were used (polyclonal unless indicated): Rac1 monoclonal (23A8, Millipore); GFAP (DAKO, Carpinteria, CA); IL-1β (H-153, Santa Cruz Biosciences, Santa Cruz, CA), and GSPT1 (10763-1-AP; Proteintech, Rosemont, IL) and eRF3 (antibody against GSPT, 14980; Cell Signaling Technology). Alexa 488-conjugated secondary antibodies were obtained from Invitrogen. HRP-conjugated GAPDH or tubulin-α antibodies were obtained from MBL International.

Plasmids and siRNA—Venus-tagged hGeminin plasmid, which is an indicator of the S-M phase and one of two components of the Fucci system (29), was provided as a kind gift from

Dr. Miyawaki (RIKEN, Wako, Japan). Human *GSPT1* cDNAs were obtained from RIKEN (Tsukuba, Japan) and cloned into pEGFP-C3 (Clontech, Mountain View, CA) and p3×FLAG-CMV-10 (Sigma-Aldrich). Myc-tagged human Rac1 plasmid and a validated target sequence of human/mouse *Rac1* for RNAi (human nucleotides 618–636 from ATG: CCTTTG-TACGCTTTGCTCA) were developed as previously described (6). shRNA expression plasmids for *Rac1* containing the validated sequence were prepared using *pSUPER*, *pSUPER(gfp)* (OrigoEngine, Seattle, WA), and *pSUPER(rfp)*, in which *gfp* of *pSUPER(gfp)* was replaced by *mCherry*. The plasmids were named *pSUPER(618)* (55), *shRac1(618gfp)*, and *shRac1(618rfp)*, respectively.

The target sequences for RNAi were CCTTTGTACGCTTT-GCTCA and GCCACTACAACAGAATTTT for human *RAC1* (618–636 and 1977–1995 from ATG, named siRac1(618) (100% conserved in mouse) and siRac1–1977, respectively), CTAAGAAAGAGCATGTAAA and GGAATCAGGATCTA-TTTGT for human *GSPT1* (620–638 and 1374–1392 from ATG, named siGSPT1–620 and siGSPT1–1374, respectively), and CCAAGAAGGAACATGTAAA for mouse *GSPT1* (620–638 from ATG, named siGSPT1(620m)). siRNAs and control siRNA (MISSION Universal Negative Control) were purchased from Sigma-Aldrich.

siRNA and shRNA plasmids were transfected into LN229 and HeLa cells using Lipofectamine 3000 (Invitrogen) or RNAiMAX (Invitrogen). siRNAs were transfected into primary astrocytes using a NEPA21 electroporator (Nepa Gene Co., Ltd., Japan). Compared with lipofection, electroporation has been reported to require a higher concentration of siRNAs (56). Thus, 20 nM siRNA was used for electroporation.

Cells—LN229 astrocytic cells and HeLa cells were maintained in DMEM (Wako) containing 10% FBS (Nichirei Biosciences, Japan). Primary astrocyte cultures were prepared from mouse cerebral cortex at postnatal day 1 or 2. Dissected cerebral cortexes were dissociated in Eagle's minimal essential medium (Wako) supplemented with 10% FBS, 100 units/ml penicillin, and 100 μg/ml streptomycin and were cultured in 25-cm^2 flasks (2 brains/flask) (Corning Inc., Corning, NY). After 5–7 days, the flasks were subjected to 2 h of continuous shaking to obtain purified astrocytes. Trypsinized cells and cell lysates were used for the experiments, as indicated (only one trypsinization step was used for the primary astrocytes). The percentage of primary astrocytes obtained from *GFAP-Cre;Rac1$^{flox/flox}$;tdTomato* mice with tdTomato fluorescence was 80–90%. All cells were maintained in a 5% CO$_2$ humidified incubator at 37 °C.

RT-PCR—RT-PCR was performed with 1 μg of total RNA obtained from the primary astrocytes of WT mice using SuperScript III reverse transcriptase (Invitrogen) and random primers. The following primer pairs were used for PCR (30 cycles): 5′-GCAGACAGACGTGTTCTTAATTTGC-3′ and 5′-TGT-AACAAAAACTTGGCATCAAATGCG-3′ for *Rac1*, 5′-GGA-GGACTATGACCGCCTC-3′ and 5′-AAATAGGATGTGGC-CTATGAACATCC-3′ for *Rac2*, and 5′-CCCACACACAC-CCATCCTTC-3′ and 5′-TGGAGCTATATCCCAGAAAA-AGGAG-3′ for *Rac3*.

Rac1-GSPT1 Signaling in Astrogliosis

Cell Cycle Analysis—LN229 and HeLa cells were cultured on 35-mm glass-bottomed dishes (gbd; MatTek, Ashland, MA). LN229 cells were transfected with Venus-tagged hGeminin + shRNA expression plasmid (pSUPER(rfp) or shRac1(618rfp)) using Lipofectamine 3000. HeLa cells were transfected with Venus-tagged hGeminin + siRNA (control or siGSPT1). For rescue experiments, HeLa cells with transfection of siRac1(618) were simultaneously transfected with pEGFP-C1 or GFP-GSPT1 using Lipofectamine 3000. Starting at 24 h after transfection, the cells were imaged every 20 min for 72 h at 37 °C in 5% CO_2 using a computer-assisted incubator fluorescence microscope system (LCV110; Olympus). This system enabled ultra long term imaging of living cells without removal of the cells from the culture conditions. LN229 cells with RFP fluorescence and HeLa cells with Venus or GFP fluorescence were analyzed as cells with shRNA or siRNA. Cell cycle (doubling time) was defined as the time from one cytokinesis to the next cytokinesis. The experiments were performed in duplicate, and at least three independent transfection experiments were conducted.

siRNA (control, siRac1(618) or siGSPT1(620m)) was electroporated into WT primary astrocytes in combination with the pEGFP-C1 plasmid. Primary astrocytes obtained from *GFAP-Cre;Rac1^{flox/flox};tdTomato* (Rac1-KO) mice and control (*Rac1^{flox/flox};tdTomato*) mice or primary astrocytes subjected to electroporation were cultured on 35-mm gbd. Starting at 48 h after plating on gbd, the cells were imaged every 20 min for 72 h using a live imaging LCV110 system, as described above. Astrocytes with tdTomato fluorescence and GFP fluorescence were considered to be Rac1-KO cells and cells containing siRNA, respectively.

Scratch Wound (Wound Healing) Assay—LN229 cells were transfected with shRNA expression plasmid (pSUPER(gfp) or shRac1(618gfp)), or pEGFP(C1) + siRNA (control or siGSPT1) using Lipofectamine 3000. At 24 h after transfection, culture media were changed to serum-free media, and cells were grown for an additional 24 h. Forty-eight hours after transfection, an approximately 1,000-μm-wide section of the cells was scratched using a sterilized 1,000-μl filter tip, and imaged every 20 min for 48 h using a live imaging LCV110 system (see the "cell cycle analysis" section for details). Cells with GFP fluorescence were analyzed as cells with shRNA or siRNA. Cells whose cell bodies has translocated were considered to be migrated cells. Cell migration was defined as the distance from the leading edge of the cell at the starting time point to the same point on the cell at the ending time point. Experiments were performed in duplicate, and at least three independent transfections were conducted.

siRNA (control, siRac1(618), or siGSPT1(620m)) was electroporated into WT primary astrocytes in combination with the pEGFP(C1) plasmid. Primary astrocytes obtained from *GFAP-Cre;Rac1^{flox/flox};tdTomato* (Rac1-KO) mice and control mice or primary astrocytes treated with electroporation were cultured on 35-mm gbd. Forty-eight hours after plating on gbd, the cells were imaged every 20 min for 72 h using a live imaging LCV110 system. Astrocytes with tdTomato fluorescence and GFP fluorescence were considered to be Rac1-KO cells and cells containing siRNA, respectively.

Cell Migration Assay—Migration of primary astrocytes was evaluated using the CytoSelect cell migration assay kit (12 μm pore size, colorimetric format; Cell Biolabs, Inc., San Diego, CA) according to the manufacturer's protocol. Briefly, 2.0 × 10^5 primary astrocytes obtained from *GFAP-Cre;Rac1^{flox/flox};tdTomato* (Rac1-KO) mice and control (*Rac1^{flox/flox};tdTomato*) mice or 5.0 × 10^5 WT primary astrocytes treated with electroporation (pEGFP-C3 + 20 nM of siRNA (control or siGSPT1(620m)) suspended in serum-free DMEM were placed in 24-well insets, and 500 μl of DMEM containing 10% FBS was added to the lower wells of the 24-well plate. After 24 h (Rac1-KO) or 32 h (GSPT1-KD), non-migrating cells on the interior surface of the inset were removed, and migrated cells on the exterior surface of the inset were stained using stain solution. After extraction of the migrated cells in extraction solution, the *A* value at 560 nm was obtained using a plate reader (Multiskan GO; Thermo Fisher Scientific). The data are shown as percentages of control.

Section Preparation and Immunohistochemistry—At 35 days after SCI and 21 days after microbeam irradiation injury, the animals were deeply anesthetized using pentobarbital and transcardially perfused with ice-cold 0.9% saline solution and then with 4% paraformaldehyde in 0.1 M phosphate buffer (pH 7.4) (57). Spinal cords and brains were dissected, post-fixed overnight in the same fresh fixative, and then embedded in paraffin. Three-μm sagittal sections of the spinal cord and cerebellum with brainstem were obtained (from 5-mm rostral and caudal to the injury site in the case of SCI). After deparaffinization and permeabilization with PBS containing 0.3% Triton X-100 (PBS-0.3T), spinal cord sections were incubated overnight with a GFAP antibody in PBS containing 0.03% Triton X-100 (PBS-0.03T) at 4 °C, followed by incubation with Alexa 488-conjugated secondary antibodies for 1 h at 24 °C. The cerebellum with brainstem sections were incubated overnight with a GFAP antibody in PBS containing 0.03% Triton X-100 (PBS-0.03T) at 4 °C, followed by diaminobenzidine staining using a Vectastain ABC kit (Vector Laboratories, Burlingame, CA) and counterstaining using Cresyl violet solution (Muto Pure Chemicals, Tokyo, Japan). Quantification of GFAP immunoreactivity was performed as follows. For SCI cases, fluorescent images were captured using a fluorescence microscopy system (Biozero, Keyence, Japan). Immunoreactivity in a 100-μm area from the lesion edge was measured using ImageJ software (National Institutes of Health, Bethesda, MD). Areas that appeared brighter than the background were defined as GFAP-positive areas. The number of pixels were calculated, and the GFAP-positive area was defined as a percentage of the number of pixels for the entire area. For microbeam irradiation injury cases, diaminobenzidine stainings were photographed using a light microscope (Axioplan II; Carl Zeiss) with a DP26 camera (Olympus). Immunoreactivity areas that appeared brighter than the background (as analyzed by ImageJ software) were defined as GFAP-positive areas, which were defined in a linear band. The region of interest (ROI) was defined as a 400-μm square with its center in the linear immunoreactivity band of the GFAP-positive area, and the GFAP-positive immunoreactivity area was calculated as a percentage of the total area.

Immunoblotting—The cells were lysed in homogenizing buffer (58) by sonication in the presence of protease inhibitor mixture, protein phosphatase inhibitor mixture (Nacalai Tesque, Tokyo, Japan), and 1% Triton X-100. Total lysates were centrifuged at $800 \times g$ for 5 min at 4 °C, and the supernatants were subjected to SDS-PAGE, followed by immunoblotting for 2 h at 24 °C using primary antibodies diluted in PBS-0.03T. The bound primary antibodies were detected with secondary Ab-HRP conjugates using the ECL detection system (GE Healthcare).

DNA Microarray—LN229 cells were transfected with *pSUPER* or *shRac(618)*. At 24 h after transfection, LN229 cells were treated with LPS (0.5 μg/ml) for 24 h, and then total RNAs were extracted using TRIzol (Invitrogen). The quality and quantity of RNA were determined using the Agilent 2100 Bio-Analyzer. Gene expression profiles were examined using the SurePrint G3 Mouse Gene Expression 8 × 60K microarray kit (Agilent Technologies, Lexington, MA).

Statistical Analysis—All data are presented as the means ± S.E. For comparisons of two groups, unpaired Student's *t* tests were used. For comparisons of more than two groups, one-way analysis of variance (ANOVA) or repeated measures two-way ANOVA was performed and followed by Bonferroni post hoc test of pairwise group differences. Statistical analyses were performed using Prism 6.0 software (GraphPad, La Jolla, CA); $p < 0.05$ was considered statistically significant.

Author Contributions—T. Uey. and N. S. planned the project. T. I., T. Uey., and T. H. performed the molecular biology experiments. M. S., T. Ku., and C. T. performed the SCI experiments. T. Ko. performed the microbeam irradiation injury experiments. M. K. and E. K. performed histological experiments. T. I., T.Uey., and T.Ueb. performed a long term, time lapse live imaging. A. A. and D. H. G. provided the animals. T. I., T. Uey., C. T., and N. S. analyzed the data, and T. Uey. wrote the manuscript.

References

1. Pekny, M., Pekna, M., Messing, A., Steinhäuser, C., Lee, J. M., Parpura, V., Hol, E. M., Sofroniew, M. V., and Verkhratsky, A. (2016) Astrocytes: a central element in neurological diseases. *Acta Neuropathol.* **131,** 323–345

2. Sofroniew, M. V. (2009) Molecular dissection of reactive astrogliosis and glial scar formation. *Trends Neurosci.* **32,** 638–647

3. Pekny, M., and Pekna, M. (2014) Astrocyte reactivity and reactive astrogliosis: costs and benefits. *Physiol. Rev.* **94,** 1077–1098

4. Wang, S., Watanabe, T., Matsuzawa, K., Katsumi, A., Kakeno, M., Matsui, T., Ye, F., Sato, K., Murase, K., Sugiyama, I., Kimura, K., Mizoguchi, A., Ginsberg, M. H., Collard, J. G., and Kaibuchi, K. (2012) Tiam1 interaction with the PAR complex promotes talin-mediated Rac1 activation during polarized cell migration. *J. Cell Biol.* **199,** 331–345

5. Bosco, E. E., Mulloy, J. C., and Zheng, Y. (2009) Rac1 GTPase: a "Rac" of all trades. *Cell Mol. Life Sci.* **66,** 370–374

6. Ueyama, T., Geiszt, M., and Leto, T. L. (2006) Involvement of Rac1 in activation of multicomponent Nox1- and Nox3-based NADPH oxidases. *Mol. Cell. Biol.* **26,** 2160–2174

7. Leto, T. L., Morand, S., Hurt, D., and Ueyama, T. (2009) Targeting and regulation of reactive oxygen species generation by Nox family NADPH oxidases. *Antioxid. Redox Signal.* **11,** 2607–2619

8. Cooney, S. J., Bermudez-Sabogal, S. L., and Byrnes, K. R. (2013) Cellular and temporal expression of NADPH oxidase (NOX) isotypes after brain injury. *J. Neuroinflammation* **10,** 155

9. Loane, D. J., Stoica, B. A., Byrnes, K. R., Jeong, W., and Faden, A. I. (2013) Activation of mGluR5 and inhibition of NADPH oxidase improves functional recovery after traumatic brain injury. *J. Neurotrauma* **30,** 403–412

10. Angeloni, C., Prata, C., Dalla Sega, F. V., Piperno, R., and Hrelia, S. (2015) Traumatic brain injury and NADPH oxidase: a deep relationship. *Oxid. Med. Cell Longev.* **2015,** 370312

11. Zhang, L., Wu, J., Duan, X., Tian, X., Shen, H., Sun, Q., and Chen, G. (2016) NADPH oxidase: a potential target for treatment of stroke. *Oxid. Med. Cell Longev.* **2016,** 5026984

12. Chen, H., Song, Y. S., and Chan, P. H. (2009) Inhibition of NADPH oxidase is neuroprotective after ischemia-reperfusion. *J. Cereb. Blood Flow Metab.* **29,** 1262–1272

13. Ozaki, M., Deshpande, S. S., Angkeow, P., Bellan, J., Lowenstein, C. J., Dinauer, M. C., Goldschmidt-Clermont, P. J., and Irani, K. (2000) Inhibition of the Rac1 GTPase protects against nonlethal ischemia/reperfusion-induced necrosis and apoptosis *in vivo*. *FASEB J.* **14,** 418–429

14. Talukder, M. A., Elnakish, M. T., Yang, F., Nishijima, Y., Alhaj, M. A., Velayutham, M., Hassanain, H. H., and Zweier, J. L. (2013) Cardiomyocyte-specific overexpression of an active form of Rac predisposes the heart to increased myocardial stunning and ischemia-reperfusion injury. *Am. J. Physiol. Heart Circ. Physiol.* **304,** H294–H302

15. Bedard, K., and Krause, K. H. (2007) The NOX family of ROS-generating NADPH oxidases: physiology and pathophysiology. *Physiol. Rev.* **87,** 245–313

16. Carrizzo, A., Forte, M., Lembo, M., Formisano, L., Puca, A. A., and Vecchione, C. (2014) Rac-1 as a new therapeutic target in cerebro- and cardiovascular diseases. *Curr. Drug. Targets* **15,** 1231–1246

17. Fujita, Y., and Yamashita, T. (2014) Axon growth inhibition by RhoA/ROCK in the central nervous system. *Front. Neurosci.* **8,** 338

18. Karimi-Abdolrezaee, S., and Billakanti, R. (2012) Reactive astrogliosis after spinal cord injury-beneficial and detrimental effects. *Mol. Neurobiol.* **46,** 251–264

19. Pekny, M., Wilhelmsson, U., and Pekna, M. (2014) The dual role of astrocyte activation and reactive gliosis. *Neurosci. Lett.* **565,** 30–38

20. Kikuchi, Y., Shimatake, H., and Kikuchi, A. (1988) A yeast gene required for the G$_1$-to-S transition encodes a protein containing an A-kinase target site and GTPase domain. *EMBO J.* **7,** 1175–1182

21. Hoshino, S., Imai, M., Mizutani, M., Kikuchi, Y., Hanaoka, F., Ui, M., and Katada, T. (1998) Molecular cloning of a novel member of the eukaryotic polypeptide chain-releasing factors (eRF): its identification as eRF3 interacting with eRF1. *J. Biol. Chem.* **273,** 22254–22259

22. Chauvin, C., Salhi, S., Le Goff, C., Viranaicken, W., Diop, D., and Jean-Jean, O. (2005) Involvement of human release factors eRF3a and eRF3b in translation termination and regulation of the termination complex formation. *Mol. Cell. Biol.* **25,** 5801–5811

23. Bajenaru, M. L., Zhu, Y., Hedrick, N. M., Donahoe, J., Parada, L. F., and Gutmann, D. H. (2002) Astrocyte-specific inactivation of the neurofibromatosis 1 gene (NF1) is insufficient for astrocytoma formation. *Mol. Cell. Biol.* **22,** 5100–5113

24. Kassai, H., Terashima, T., Fukaya, M., Nakao, K., Sakahara, M., Watanabe, M., and Aiba, A. (2008) Rac1 in cortical projection neurons is selectively required for midline crossing of commissural axonal formation. *Eur. J. Neurosci.* **28,** 257–267

25. Basso, D. M., Fisher, L. C., Anderson, A. J., Jakeman, L. B., McTigue, D. M., and Popovich, P. G. (2006) Basso Mouse Scale for locomotion detects differences in recovery after spinal cord injury in five common mouse strains. *J. Neurotrauma* **23,** 635–659

26. Teshigawara, K., Kuboyama, T., Shigyo, M., Nagata, A., Sugimoto, K., Matsuya, Y., and Tohda, C. (2013) A novel compound, denosomin, ameliorates spinal cord injury via axonal growth associated with astrocyte-secreted vimentin. *Br. J. Pharmacol.* **168,** 903–919

27. Uyama, A., Kondoh, T., Nariyama, N., Umetani, K., Fukumoto, M., Shinohara, K., and Kohmura, E. (2011) A narrow microbeam is more effective for tumor growth suppression than a wide microbeam: an *in vivo* study using implanted human glioma cells. *J. Synchrotron Radiat.* **18,** 671–678

28. Nariyama, N., Ohigashi, T., Umetani, K., Shinohara, K., Tanaka, H., Maruhashi, A., Kashino, G., Kurihara, A., Kondob, T., Fukumoto, M., and Ono, K. (2009) Spectromicroscopic film dosimetry for high-energy microbeam from synchrotron radiation. *Appl. Radiat. Isot.* **67,** 155–159

29. Sakaue-Sawano, A., Kurokawa, H., Morimura, T., Hanyu, A., Hama, H., Osawa, H., Kashiwagi, S., Fukami, K., Miyata, T., Miyoshi, H., Imamura, T., Ogawa, M., Masai, H., and Miyawaki, A. (2008) Visualizing spatiotemporal dynamics of multicellular cell-cycle progression. *Cell* **132,** 487–498

30. Hsu, H. Y., and Wen, M. H. (2002) Lipopolysaccharide-mediated reactive oxygen species and signal transduction in the regulation of interleukin-1 gene expression. *J. Biol. Chem.* **277,** 22131–22139

31. Pineau, I., and Lacroix, S. (2007) Proinflammatory cytokine synthesis in the injured mouse spinal cord: multiphasic expression pattern and identification of the cell types involved. *J. Comp Neurol* **500,** 267–285

32. Denes, A., Wilkinson, F., Bigger, B., Chu, M., Rothwell, N. J., and Allan, S. M. (2013) Central and haematopoietic interleukin-1 both contribute to ischaemic brain injury in mice. *Dis. Model. Mech.* **6,** 1043–1048

33. Okada, S., Nakamura, M., Katoh, H., Miyao, T., Shimazaki, T., Ishii, K., Yamane, J., Yoshimura, A., Iwamoto, Y., Toyama, Y., and Okano, H. (2006) Conditional ablation of Stat3 or Socs3 discloses a dual role for reactive astrocytes after spinal cord injury. *Nat. Med.* **12,** 829–834

34. Herrmann, J. E., Imura, T., Song, B., Qi, J., Ao, Y., Nguyen, T. K., Korsak, R. A., Takeda, K., Akira, S., and Sofroniew, M. V. (2008) STAT3 is a critical regulator of astrogliosis and scar formation after spinal cord injury. *J. Neurosci.* **28,** 7231–7243

35. Brennan, F. H., Gordon, R., Lao, H. W., Biggins, P. J., Taylor, S. M., Franklin, R. J., Woodruff, T. M., and Ruitenberg, M. J. (2015) The complement receptor C5aR controls acute inflammation and astrogliosis following spinal cord injury. *J. Neurosci.* **35,** 6517–6531

36. Bardehle, S., Krüger, M., Buggenthin, F., Schwausch, J., Ninkovic, J., Clevers, H., Snippert, H. J., Theis, F. J., Meyer-Luehmann, M., Bechmann, I., Dimou, L., and Götz, M. (2013) Live imaging of astrocyte responses to acute injury reveals selective juxtavascular proliferation. *Nat. Neurosci.* **16,** 580–586

37. Heasman, S. J., and Ridley, A. J. (2008) Mammalian Rho GTPases: new insights into their functions from *in vivo* studies. *Nat. Rev. Mol. Cell Biol.* **9,** 690–701

38. Nakayama, M., Goto, T. M., Sugimoto, M., Nishimura, T., Shinagawa, T., Ohno, S., Amano, M., and Kaibuchi, K. (2008) Rho-kinase phosphorylates PAR-3 and disrupts PAR complex formation. *Dev. Cell* **14,** 205–215

39. Michaelson, D., Abidi, W., Guardavaccaro, D., Zhou, M., Ahearn, I., Pagano, M., and Philips, M. R. (2008) Rac1 accumulates in the nucleus during the G_2 phase of the cell cycle and promotes cell division. *J. Cell Biol.* **181,** 485–496

40. Davies, T., and Canman, J. C. (2012) Stuck in the middle: Rac, adhesion, and cytokinesis. *J. Cell Biol.* **198,** 769–771

41. Yoshida, T., Zhang, Y., Rivera Rosado, L. A., Chen, J., Khan, T., Moon, S. Y., and Zhang, B. (2010) Blockade of Rac1 activity induces G_1 cell cycle arrest or apoptosis in breast cancer cells through downregulation of cyclin D1, survivin, and X-linked inhibitor of apoptosis protein. *Mol. Cancer Ther.* **9,** 1657–1668

42. Liu, L., Zhang, H., Shi, L., Zhang, W., Yuan, J., Chen, X., Liu, J., Zhang, Y., and Wang, Z. (2014) Inhibition of Rac1 activity induces G_1/S phase arrest through the GSK3/cyclin D1 pathway in human cancer cells. *Oncol. Rep.* **32,** 1395–1400

43. Joyce, D., Bouzahzah, B., Fu, M., Albanese, C., D'Amico, M., Steer, J., Klein, J. U., Lee, R. J., Segall, J. E., Westwick, J. K., Der, C. J., and Pestell, R. G. (1999) Integration of Rac-dependent regulation of cyclin D1 transcription through a nuclear factor-κB-dependent pathway. *J. Biol. Chem.* **274,** 25245–25249

44. Pedersen, E., Wang, Z., Stanley, A., Peyrollier, K., Rösner, L. M., Werfel, T., Quondamatteo, F., and Brakebusch, C. (2012) RAC1 in keratinocytes regulates crosstalk to immune cells by Arp2/3-dependent control of STAT1. *J. Cell Sci.* **125,** 5379–5390

45. Chauvin, C., Salhi, S., and Jean-Jean, O. (2007) Human eukaryotic release factor 3a depletion causes cell cycle arrest at G_1 phase through inhibition of the mTOR pathway. *Mol. Cell. Biol.* **27,** 5619–5629

46. Nair, S., Bora-Singhal, N., Perumal, D., and Chellappan, S. (2014) Nicotine-mediated invasion and migration of non-small cell lung carcinoma cells by modulating STMN3 and GSPT1 genes in an ID1-dependent manner. *Mol. Cancer* **13,** 173

47. Xiao, R., Li, C., and Chai, B. (2015) miRNA-144 suppresses proliferation and migration of colorectal cancer cells through GSPT1. *Biomed. Pharmacother.* **74,** 138–144

48. Mack, N. A., Whalley, H. J., Castillo-Lluva, S., and Malliri, A. (2011) The diverse roles of Rac signaling in tumorigenesis. *Cell Cycle* **10,** 1571–1581

49. Yukinaga, H., Shionyu, C., Hirata, E., Ui-Tei, K., Nagashima, T., Kondo, S., Okada-Hatakeyama, M., Naoki, H., and Matsuda, M. (2014) Fluctuation of Rac1 activity is associated with the phenotypic and transcriptional heterogeneity of glioma cells. *J. Cell Sci.* **127,** 1805–1815

50. Hodis, E., Watson, I. R., Kryukov, G. V., Arold, S. T., Imielinski, M., Theurillat, J. P., Nickerson, E., Auclair, D., Li, L., Place, C., Dicara, D., Ramos, A. H., Lawrence, M. S., Cibulskis, K., Sivachenko, A., *et al.* (2012) A landscape of driver mutations in melanoma. *Cell* **150,** 251–263

51. Krauthammer, M., Kong, Y., Ha, B. H., Evans, P., Bacchiocchi, A., McCusker, J. P., Cheng, E., Davis, M. J., Goh, G., Choi, M., Ariyan, S., Narayan, D., Dutton-Regester, K., Capatana, A., Holman, E. C., *et al.* (2012) Exome sequencing identifies recurrent somatic RAC1 mutations in melanoma. *Nat. Genet.* **44,** 1006–1014

52. Kawazu, M., Ueno, T., Kontani, K., Ogita, Y., Ando, M., Fukumura, K., Yamato, A., Soda, M., Takeuchi, K., Miki, Y., Yamaguchi, H., Yasuda, T., Naoe, T., Yamashita, Y., Katada, T., *et al.* (2013) Transforming mutations of RAC guanosine triphosphatases in human cancers. *Proc. Natl. Acad. Sci. U.S.A.* **110,** 3029–3034

53. Litchfield, K., Holroyd, A., Lloyd, A., Broderick, P., Nsengimana, J., Eeles, R., Easton, D. F., Dudakia, D., Bishop, D. T., Reid, A., Huddart, R. A., Grotmol, T., Wiklund, F., Shipley, J., Houlston, R. S., *et al.* (2015) Identification of four new susceptibility loci for testicular germ cell tumour. *Nat. Commun* **6,** 8690

54. Cooney, S. J., Zhao, Y., and Byrnes, K. R. (2014) Characterization of the expression and inflammatory activity of NADPH oxidase after spinal cord injury. *Free Radic. Res.* **48,** 929–939

55. Shirafuji, T., Ueyama, T., Yoshino, K., Takahashi, H., Adachi, N., Ago, Y., Koda, K., Nashida, T., Hiramatsu, N., Matsuda, T., Toda, T., Sakai, N., and Saito, N. (2014) The role of Pak-interacting exchange factor-β phosphorylation at serines 340 and 583 by PKCγ in dopamine release. *J. Neurosci.* **34,** 9268–9280

56. Ovcharenko, D., Jarvis, R., Hunicke-Smith, S., Kelnar, K., and Brown, D. (2005) High-throughput RNAi screening *in vitro*: from cell lines to primary cells. *RNA* **11,** 985–993

57. Ueyama, T., Ren, Y., Sakai, N., Takahashi, M., Ono, Y., Kondoh, T., Tamaki, N., and Saito, N. (2001) Generation of a constitutively active fragment of PKN in microglia/macrophages after middle cerebral artery occlusion in rats. *J. Neurochem.* **79,** 903–913

58. Ueyama, T., Ninoyu, Y., Nishio, S. Y., Miyoshi, T., Torii, H., Nishimura, K., Sugahara, K., Sakata, H., Thumkeo, D., Sakaguchi, H., Watanabe, N., Usami, S. I., Saito, N., and Kitajiri, S. I. (2016) Constitutive activation of DIA1 (DIAPH1) via C-terminal truncation causes human sensorineural hearing loss. *EMBO Mol. Med.* **8,** 1310–1324